Advances in Civil Engineering

WILEY

RESEARCH ARTICLE OPEN ACCESS

# Effectiveness of Nourishment and Mega-Nourishment Interventions in Macro-Tidal Coastal Environments

Nicoletta Leonardi[1] | Iacopo Carnacina[2]

[1]Department of Geography and Planning, University of Liverpool, Liverpool, UK | [2]School of Civil Engineering and Built Environment, Liverpool John Moores University, Liverpool, UK

**Correspondence:** Nicoletta Leonardi (nicleona@liverpool.ac.uk)

**Received:** 20 March 2025 | **Revised:** 2 April 2026 | **Accepted:** 7 April 2026

**Academic Editor:** Arnab Biswas

## ABSTRACT

Large-scale nourishments and mega-nourishments are increasingly employed as nature-based solutions (NBS) to enhance coastal resilience. This study evaluates the hydrodynamic effects of nourishments and mega-nourishments of varying radius (500 m–2 km) and elevation (2–3 m) in a macro-tidal embayment in the United Kingdom, Morecambe Bay, using a hydrodynamic model developed in Delft3D. Offshore wave heights of 0.5–1 m were applied at the open boundary. The analysis focuses on the capacity of these interventions to dissipate wave energy and reduce water levels under typical offshore conditions. For the largest interventions, the results indicate wave height reductions within the nourished area of up to 0.7 m and maximum water level decreases of up to 0.8 m. For the smaller radius (500 m), increasing the footprint generally produced significantly greater reductions than increasing elevation alone, whereas at a radius of 1.5 km, the results were more variable. Higher offshore wave conditions further enhanced the dissipation effect. Changes outside the intervention were comparatively minor, reflecting localised energy dissipation via depth-limited breaking and bottom friction. Sediment transport and morphological changes were not included in this analysis, which should be considered when interpreting the results. Although in some cases, absolute reductions remain modest, they can be relevant for hydraulic loading on both the nourishment and adjacent infrastructure, with potential benefits for overtopping, operational performance, and long-term maintenance.

## 1 | Introduction

At present, numerous coastal infrastructures, including power stations, railway networks, wastewater treatment facilities and millions of properties, are increasingly vulnerable to coastal flooding and erosion. The economic feasibility of traditional hard engineering solutions is becoming increasingly challenging due to the substantial costs associated with construction, maintenance and adaptation to rising sea levels and intensifying storm events. In the UK, for instance, the projected cost of realigning traditional coastal defences, such as seawalls, to safeguard coastal infrastructure against sea level rise is expected to increase by between 150% and 400% by the end of the century (e.g., [1]).

There has been a growing interest in nature-based solutions (NBS) and hybrid interventions, which include the establishment of salt marshes, seagrass beds, beach nourishment and large-scale mega-nourishment schemes. These approaches often represent more economically viable alternatives while also delivering additional benefits, such as biodiversity enhancement and the creation of recreational spaces [2–4]. The successful and widespread adoption of NBS depends on a rigorous evaluation of their performance under varying environmental conditions and climate change scenarios, as well as their capacity to dissipate wave energy and influence surrounding hydrodynamics and morphological evolution (e.g., [5–7]).

In addition to technical feasibility, the uptake of these solutions is contingent upon societal and stakeholder acceptance. Using survey data, Pannozzo and Leonardi [8] evaluated technical experts' and community members' knowledge and perceptions of NBS for coastal protection across multiple European countries. Among technical experts, higher knowledge was linked to greater awareness of potential applications, while community members showed more limited technical understanding compared to sector experts but generally supported sustainable and eco-friendly management practices. Schuerch et al. [9] highlight challenges associated with the implementation of managed realignment interventions, which involve the inland repositioning of existing sea defences to create intertidal habitats, primarily salt marshes. Such interventions often face considerable opposition due to the necessity of surrendering previously cultivated or inhabited land to the sea. Furthermore, cultural and socioeconomic factors, alongside scepticism regarding the efficacy of NBS, can contribute to resistance [9–12].

A notable large-scale NBS is the Sand Motor in the Netherlands, which is often cited as a flagship initiative for mega-nourishments. The Sand Motor, implemented in 2011 as a single large-scale mega-nourishment comprising around 21 million $m^3$ of sand, was designed to reduce the frequency of nourishment interventions and extend the lifespan of the nourishment itself [13, 14]. It was initially intended to function for at least 20 years based on an estimated annual sediment loss of 0.8–1.0 million $m^3$ [15]. More recent updates suggest that the intervention is expected to last longer, with a projected lifespan of the order of 30 years (https://www.rijkswaterstaat.nl/en/projects/iconic-structures/the-sand-motor?). Roest et al. [16] conducted a detailed morphological analysis of the Sand Motor using three bathymetric datasets spanning the period from 2011 to 2017. Their study highlighted the rapid morphological evolution of the intervention, demonstrating that it significantly altered the sediment budget along a substantial stretch of the shoreline. Over time, the Sand Motor migrated towards a Gaussian shape. The mean sea-level isobath exhibited the most pronounced morphological changes, with a retreat of ~400 m at a rate of 80 m/year. Conversely, the −10 m isobath (relative to the Dutch ordnance level, approximately MSL) remained relatively stable. Further investigation by Luijendijk et al. [17] revealed that erosion of the Sand Motor was linearly correlated with the cumulative wave energy of individual high-energy events. Their findings suggested that storm duration exerted a greater influence on erosion than maximum wave height, while wave direction (dir) had little bearing on the overall erosion trend.

In the Netherlands, between 1970 and 1990, the average annual nourished volume was 3.5 million $m^3$. From 1990, proactive nourishment became part of a dynamic coastline management strategy, increasing the average annual volume to 6.4 million $m^3$ for routine maintenance. By 2000, this further rose to 12 million $m^3$ per year for regular coastline upkeep [18]. The average volume of a beach nourishment in the area is 0.5 million $m^3$, while shoreface nourishments typically involve 1.6 million $m^3$. Channel wall nourishments, placed on the landward side of a channel, have also been implemented with volumes ranging from 1 to 6.3 million $m^3$ [18]. Beach nourishments normally have the shortest lifespan (~3 years) and deliver sand directly where it is most needed for the dynamic conservation of the coastline. Shoreface nourishments have a longer lifespan (4–10 years), although it may take several years before their effects on the shoreline position become apparent. Channel wall nourishments exhibit the longest lifespan (at least 10–15 years), and their impact on the coastline is highly variable, depending on both the nourishment design and the regional setting.

In terms of when a nourishment is classified as a mega-nourishment, it is generally assumed that such interventions involve volumes on the order of tens of millions of cubic metres, have a lifespan exceeding a decade, and are designed to replace routine annual nourishments with a single, large-scale intervention.

Tonnon et al. [19] conducted numerical modelling to establish life cycle estimates for sand-nourishment interventions, testing 10 scenarios with wave heights ranging from ~0.8 to 2 m, peak periods between 5 and 7 s, and wave dirs varying between 240° and 350°. Their findings indicated a linear relationship between the half-life of the nourishment and its initial volume, with the intervention's longevity being primarily influenced by its seaward extent and highly sensitive to wave intensity. The dominant controlling factors were identified as wave climate and longshore transport intensity. The influence of wave dir was excluded as erosion on one side of the nourishment may be counterbalanced by deposition on the other in cases of oblique wave approach.

The Environment Agency's Unit Cost Database (2007 version) provides a cost curve for beach recharge, detailing the cost per cubic metre of sand/shingle, which ranged from £8 to £21/$m^3$ (2007 prices, Report SC080039/R7). Furthermore, the cost estimation for coastal protection (Report SC080039/R7) offers the costs of several beach recharge and recycling schemes, which ranged from 50,000 to 689,000 $m^3$, with a cost per cubic metre ranging from £9 to £32/$m^3$ [20].

The implementation of mega-nourishment interventions and salt marsh restoration requires large spatial scales to ensure effectiveness. Consequently, careful evaluation of the shape and placement of such interventions is essential. Globally, increasing evidence supports the efficacy of various NBS based on site-specific case studies, contributing to a growing body of research advocating for their wider application (e.g., www.omreg.net). However, significant uncertainties remain regarding the overall effectiveness of these large-scale interventions, necessitating further studies to refine the selection of optimal coastal management strategies. This study seeks to address some of these challenges by focusing on large-scale nourishments and mega-nourishments and systematically assessing the effectiveness of different intervention designs based on their size and location within a macro-tidal setting. The research examines a macro-tidal embayment, Morecambe Bay, UK, employing numerical modelling, as outlined in Section 2, to evaluate variations in wave heights and water levels before and after the implementation of different sand-engine designs.

To date, mega-nourishment research has frequently focused on analyses of morphological evolution and sediment redistribution at specific sites and for given shapes and sizes of the interventions. Less attention has been given to systematically quantifying the short-term hydrodynamic attenuation capacity of alternative mega-nourishment geometries, particularly in macro-tidal systems. This study addresses this gap. Rather than evaluating long-term morphological evolution, the present work systematically quantifies changes in significant wave height and water levels immediately following implementation under controlled forcing conditions. The underlying assumption is that the initial stage of sand nourishment implementation represents the condition with the maximum volume of sand on the site and, potentially, the highest efficiency in terms of on-site wave energy dissipation. This approach allows for: (i) isolation of hydrodynamic response from morphodynamic feedbacks: morphological change is intentionally suppressed to isolate first-order hydrodynamic effects, enabling direct assessment of how geometry alone controls wave attenuation and water-level response. (ii) Systematic comparison of multiple idealised geometries: Instead of analysing a single implemented nourishment, this study evaluates 278 controlled simulations spanning variations in radius, elevation, wave forcing, and 23 coastal locations. This ensemble-based approach enables the identification of geometric controls on intervention effectiveness. (iii) Application in a macro-tidal environment: existing mega-nourishment studies largely examine wave-dominated micro- to meso-tidal coasts. This work instead focuses on a macro-tidal embayment (Morecambe Bay, UK), where the tidal range strongly modulates hydrodynamic response.

The article is structured as follows: Section 2 provides details on the study site and model setup, while Section 3 presents key modelling outcomes, specifically focusing on changes in wave height and water levels pre- and post-implementation of a sand engine intervention. Wave height and water levels were monitored both within and outside the sand engine. The conclusion sections summarise the key findings of the study.

## 2 | Methods

Morecambe Bay opens southwest and is a macro-tidal system with a spring tidal amplitude of up to 10 m (Figure 1). Fetch lengths are limited by the landmasses of the Isle of Man, Ireland and Spits at the Bay mouth. The significant wave height has been estimated to be around 0.5 m for 75% of the year and 2 m at the mouth of the Bay for 10% of the year [21–24]. Recent assessments of the UK wave climate indicate no clear, systematic long-term trend in significant wave height associated with climate change. Observed trends in storms and waves cannot be robustly attributed to climate change due to high interannual and decadal variability and an incomplete understanding of driving mechanisms. More broadly, analyses over the past ~30 years show spatially mixed patterns, with mean significant wave height decreasing in parts of northern UK waters and increasing in southern regions. Reported trends are generally small for the study area (on the

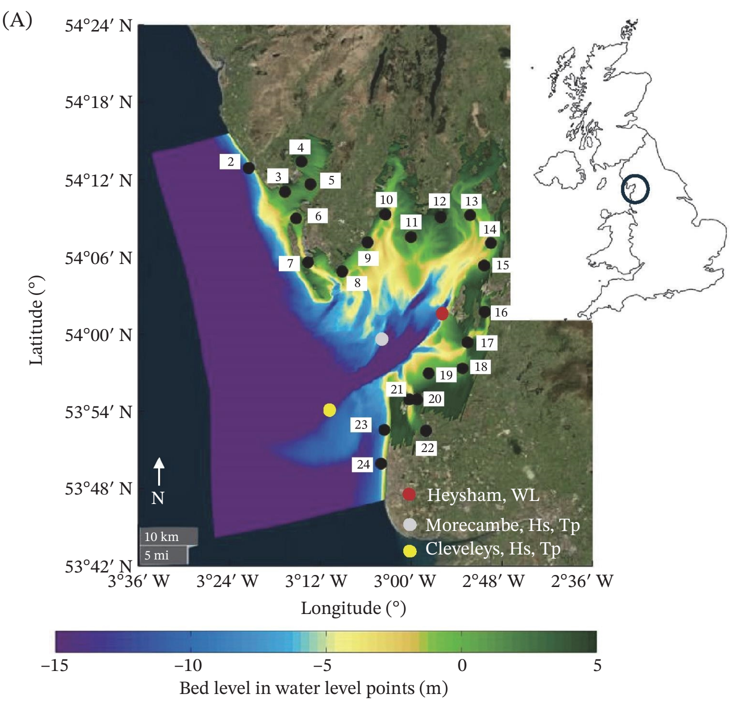


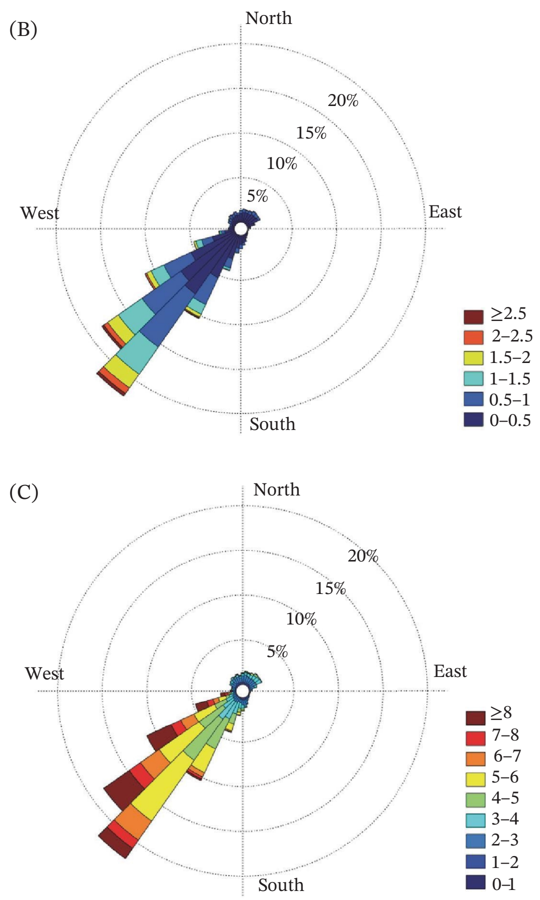


(D)

| | | |
|---|---|---|
| Locations of sand engine | 23 | (See circles (A)) |
| Radius of sand engine (m) | 500, 1500, 2000 | |
| Bathymetric changes (m) | 2, 3 | This is an increased elevation applied to every cell within a certain radius. |
| Hs (m) tested for all sand engines | 0.5, 1 | |

**FIGURE 1** | (A) Study site, Morecambe Bay, UK. Colours represent the site bathymetry (data from Edina Marine Digimap) and black circles and numbered locations represent the sites of the tested mega-nourishment interventions. Three coloured dots on the map represent the stations used for model validation: Heysham (water levels), Morecambe (waves) and Cleveleys (waves). The circle on the subpart presenting a map of the UK indicates the location of Morecambe Bay. (B and C) represent a wave rose (wave height (B) and period (C)) for the Morecambe Bay station for the year 2018. (D) Table provides a summary of all 278 numerical simulations (23 locations for 3 radii for 2 sand engine elevations for 2 wave heights and base scenarios).

order of ±2 cm per year depending on location and dataset, e.g., [25]). The bay morphodynamics and transport patterns are predominantly influenced by tidal currents and residual transport patterns even if wave presence can significantly enhance the amount of sediment in suspension [21, 26]. Large portions of the Bay are covered in fine sand [21]. The numerical model used in this study is Delft3D. Delft3D was selected due to its widespread application and validation in coastal and estuarine hydrodynamic modelling, particularly for coupled wave–current interactions in shallow-water environments. Alternative modelling frameworks (e.g., MIKE, TELEMAC, FVCOM and ROMS) could similarly be employed for this type of process-based analysis and would be expected to reproduce comparable results as they are based on comparable formulations and apply similar physical parameterisations (e.g., [27–29]). The modules Delft3D-FLOW and Delft3D-WAVE were used. The model grid resolution varies from around 90 m × 200 m to around 1000 m × 300 m offshore. The same grid was used for the FLOW and WAVE modules. Bathymetry data are based on tiles with a size of 30 m × 30 m of the product Arcsecond Gridded Bathymetry, retrieved from the EDINA Marine Digimap download service (http://digimap.edina.ac.uk/). Information on the modelling framework Delft3D can be found in Delft3 [30]. Delft3D solves the non-linear shallow water equations, which are derived from the three-dimensional Navier–Stokes equations for incompressible free-surface flow. The offshore boundary includes 10 tidal harmonics (M2, S2, N2, K2, K1, O1, P1, Q1, S1 and M4) interpolated across two boundary extremes which were derived using the global tidal model GOT-e 4.10c [31, 32], while for the two lateral boundaries, a Neumann boundary condition was imposed and set to zero for water levels. The model calibration was done using OpenDA, an open-source software framework that enables data assimilation and parameter calibration for numerical models (https://openda.org/), and by comparing the modelled tidal levels with tidal levels from the tidal station at Heysham (54.03183 latitude and −2.92025 longitude) by allowing constrained changes in bottom roughness, boundary conditions and water depth. Model performance was then evaluated using the Skill Score (BSS score) [33, 34], defined as follows:

$$\mathrm{BSS} = \frac{\alpha - \beta - \gamma + \varepsilon}{1 + \varepsilon},$$

where

$$\alpha = r_{xy}^2,\ \beta = \left(r_{xy} - \frac{\sigma_y}{\sigma_x}\right)^2,\ \gamma = \left(\frac{\langle Y \rangle - \langle X \rangle}{\sigma_x}\right)^2,\ \varepsilon = \left(\frac{X}{\sigma_x}\right)^2$$

where $r$ is the correlation coefficient, $\sigma$ is the standard deviation, $\varepsilon$ is a normalisation term and $X$ and Y are the observed and modelled values, respectively. Additional metrics are also used to evaluate model performance, including $r_{XY}^2$, RMSE, bias and the Willmott Index of Agreement. The Willmot Index of Agreement is defined as follows:

$$d = 1 - \frac{\sum_{i=1}^{n} (Y_i - X_i)}{\sum_{i=1}^{n} (|Y_i - \langle X \rangle| + |X_i - \langle X \rangle|)}.$$

The Brier Skill Score achieved for the calibrated water levels is 0.98 for water levels, the Willmott Index of Agreement is 0.99, $r_{XY}^2$ is 0.97, RMSE is 0.4181 m and bias is −0.1060 (Figure 2).

The wave conditions used for the evaluation of model performance are from the Cleveleys and Morecambe Bay wave stations (Figures 1 and 3). Wave data were obtained from the Channel Coastal Observatory website. For Morecambe Bay, the minimum and maximum longitudes are −3.06705 and −3.06505 and the minimum and maximum latitudes are 53.98919 and 53.98719, respectively. For the Cleveleys monitoring station, the minimum and maximum longitudes are −3.19683 and −3.19483 respectively, and the minimum and maximum latitudes are 53.89613 and 53.89413, respectively. The time series at Cleveleys was applied at the model's open boundaries because no wave buoys were available at the exact boundary locations. Adjusting the wave height by 20% to account for wave dissipation between the buoy and the model domain resulted in acceptable model performance. The performance of the model for the simulation of waves is present in Figure 3 and Table 1. The wave model calibration for Morecambe and Cleveleys shows generally high BSS and d index agreement for all parameters. Significant wave height (Hs) and wave period (T) have a high BSS (0.94–0.99) and index of agreement ($d$ = 0.87–0.94), indicating that the model captures both the variability and magnitude of observed waves accurately. The RMSE values for Hs are <0.5 m, and bias is negligible (±0.07 m), demonstrating low systematic errors. For T, RMSE around 1 s and moderate negative bias are within

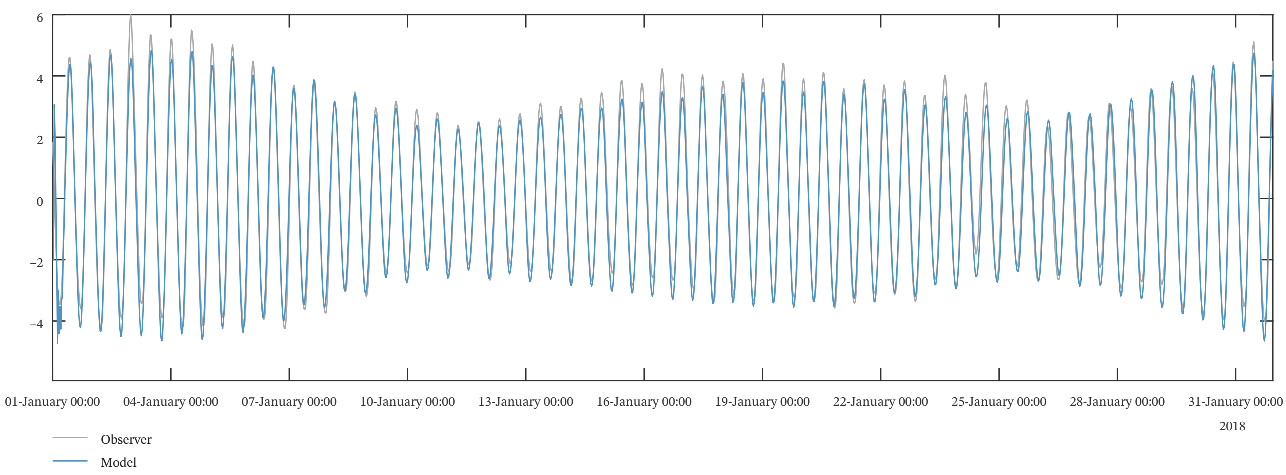


**FIGURE 2** | Simulated data and tidal buoy data from January 1st to February 1st.

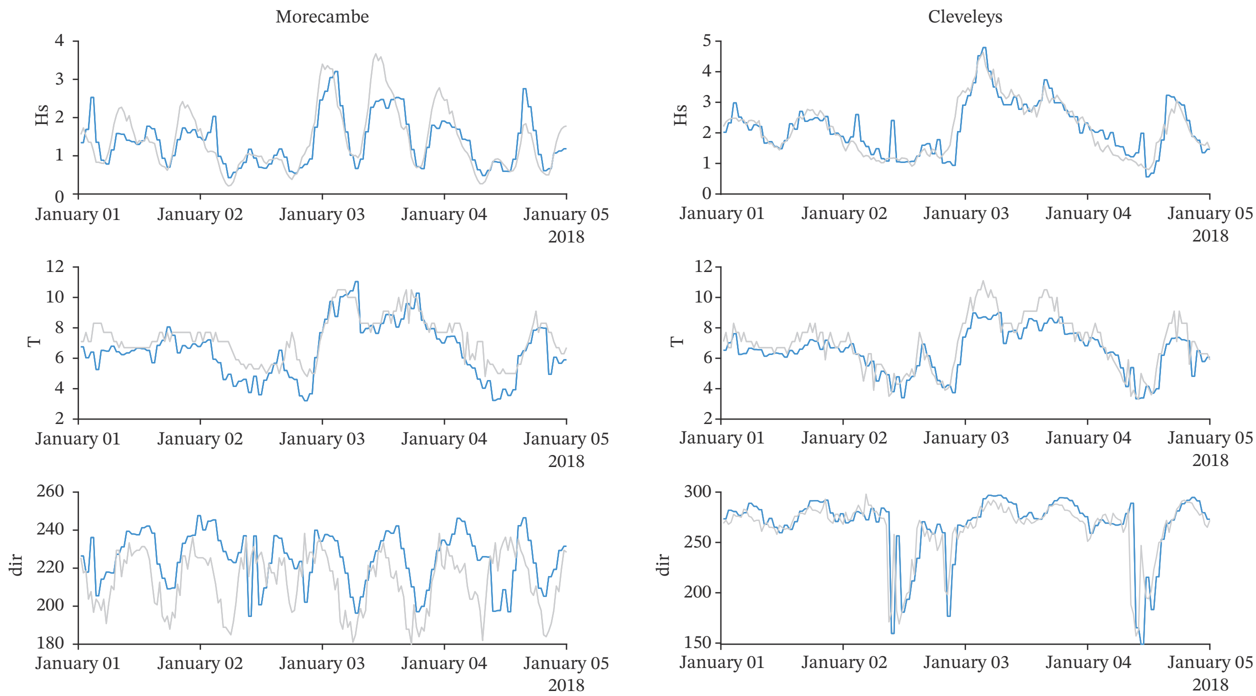


**FIGURE 3** | Wave height, wave period and wave direction for two monitoring stations (Morecambe and Cleveleys). Grey lines represent observed data at the wave buoys, while blue lines are Delft3D data. The location of the monitoring stations is present in Figure 1.

**TABLE 1** | Model metrics.

| Variable | BSS | *d* | $r^2_{XY}$ | RMSE | bias |
|---|---|---|---|---|---|
| Morecambe | | | | | |
| Hs | 0.94 | 0.90 | 0.70 | 0.45 | −0.07 |
| T | 0.95 | 0.87 | 0.77 | 1.16 | −0.73 |
| dir | 0.98 | 0.59 | 0.16 | 20.05 | 11.90 |
| Cleveleys | | | | | |
| Hs | 0.99 | 0.94 | 0.78 | 0.41 | 0.04 |
| T | 0.97 | 0.89 | 0.77 | 1.01 | −0.52 |
| dir | 0.94 | 0.83 | 0.5 | 23.3 | 2.9 |

acceptable limits. For wave heights (Hs) below 1 m, RMSE values reduce to 0.28 m for Morecambe Bay. Wave dir shows lower skill, particularly at Morecambe ($R^2 = 0.16$), with a higher RMSE and some directional bias. However, directional errors are common in nearshore and complex coastal regions due to the local bathymetry, wind variability, and boundary effects. At Cleveleys, the wave dir is moderately well captured ($R^2 = 0.50$, $d = 0.83$), suggesting that the model is still able to reproduce the dominant directional patterns.

Overall, the model's performance is considered acceptable within the scope of this article, as idealised wave boundary conditions, rather than full time-series data, are used, and the focus of the results is on comparative simulations with identical boundary conditions but differing morphologies.

The morphological factor for the model was kept at zero, and as such, there is no morphological evolution. The model bathymetry was modified to reflect the presence of different large-scale interventions and to systematically test the influence of these on waves and water level dissipation. Specifically, such modifications were introduced along the land boundary by changing the bathymetry within circular areas of varying radius (0.5, 1.5 and 2 km radius) located at regular intervals along the coastline and having elevations of 2 and 3 m above the original bathymetry. Some portions of the morphological variations were not impacting the hydrodynamics at all as they were overlapping emerged areas. For example, in the case of intervention 2 (Figure 1), portions of the north-eastern section of the intervention lie within an area that remains emergent throughout the tidal cycle (water depth equal to zero). Consequently, the effective bathymetric interaction with the flow field during the majority of the tidal period is closer to a semi-circular planform. This configuration is consistent with several of the other simulated interventions and reflects some real-world deployment features. The size and variations in elevation of the interventions were chosen to encompass orders of magnitude comparable to the one of the Netherlands Sand Motor while also covering a wider set of conditions to explore trends in the results up to the most extreme idealised case with an intervention size of 2 km radius and 3 m depth variations. Separate numerical simulations were conducted for each nourishment configuration. For each location, six interventions and a base case were thus simulated. In terms of boundary conditions, two wave conditions were tested with a significant wave height at the ocean boundary of 0.5 and 1 m and a 235° dir (Figure 1). The prevailing offshore wave climate is strongly dominated by waves approaching from ~235°, with relatively limited directional variability. This directional consistency, compared with the coastline orientation, supports the use of a representative dominant approach angle for the purposes of controlled comparison. These conditions fit within the range of values illustrated in the wave rose in Figure 1 (data obtained from the Northwest Regional Coastal Monitoring Programme, Morecambe Bay station). The forcing conditions selected in this study are intended to represent typical hydrodynamic behaviour in the system, rather than extreme or event-scale responses, and are appropriate for the study's process-based objectives. The model experiments were not intended to reproduce a specific year. Instead, they simulate typical wave conditions to enable a comparative, process-based assessment. Waves were imposed at the southwest ocean boundary using a default JONSWAP spectrum. Therefore, there were 12 ensembles (3 radii, 2 heights, 2 wave conditions), each containing 23 simulations (23 different locations). Waves and water level conditions for each intervention were monitored for two tidal cycles and through regularly spaced observation points located in the interior and exterior of the intervention at $\pm 1/3$ of the intervention radius (Figure 4).

## 3 | Results and Discussions

Figure 4 presents a time series of significant wave height for a representative intervention with a radius of 2 km, an elevation of 3 m and a boundary significant wave height of 1 m, alongside a selected set of observation points. An overview of the wave field evolution throughout the tidal cycle for this test case is provided in Supporting Information 1 Figure S1. Additionally, Figure 4 offers a representative depiction of the distribution of observation points both within and beyond the mega-nourishment intervention (zoomed section, Figure 4A).

Figure 4B–G illustrate significant wave heights at observation points located within the intervention, while Figure 4H–K pertains to those located outside the intervention. Light-blue and dark-blue lines denote conditions before and after the implementation of the intervention, respectively. As anticipated, the most pronounced changes in significant wave height occur within the intervention. In contrast, regions outside the mega-nourishment (e.g., empty diamonds) exhibit more modest variations in significant wave height.

Owing to the macro-tidal nature of the system, the most substantial changes take place at high tide, whereas periods from low tide to mean sea level remain largely unaffected by the intervention, as indicated by the cyclic wave pattern in Figure 4. Finally, the development of waves within the intervention is temporally delayed throughout the tidal cycle due to the postponed submergence of the area (e.g., Figure 4F).

Figure 5 displays the maximum significant wave height dissipation (i.e., the difference between the maximum significant wave height before and after the intervention) recorded at any observation point within the intervention (Figure 5A–C) or outside the intervention (Figure 5D–F) for each intervention location, as

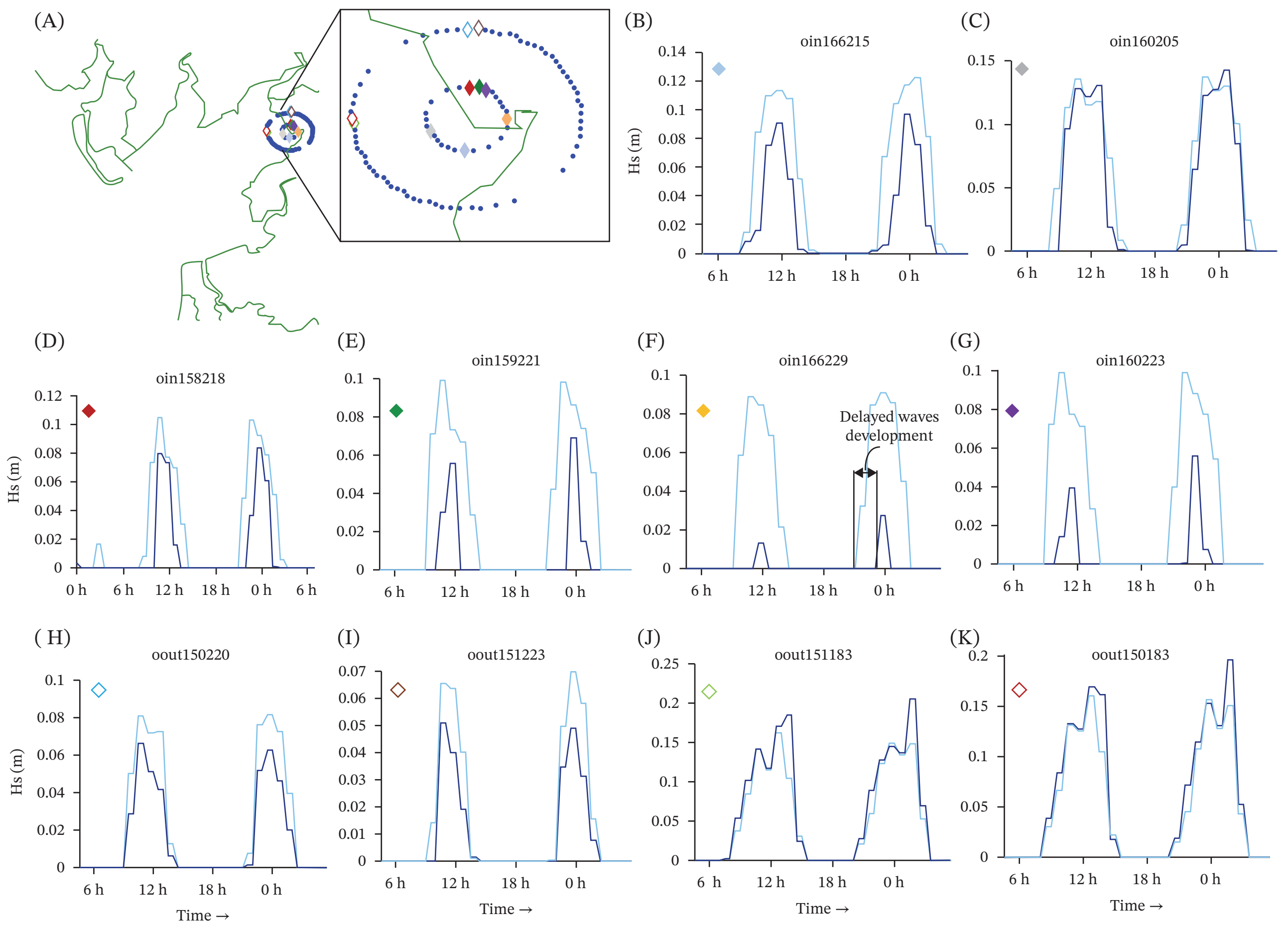


**FIGURE 4** | Time series of significant wave height (B–K) at different observation points located within and outside the management intervention (A). Empty diamonds refer to subparts presenting results for observation points outside the nourishment. Filled diamonds refer to observation points inside the nourishment.

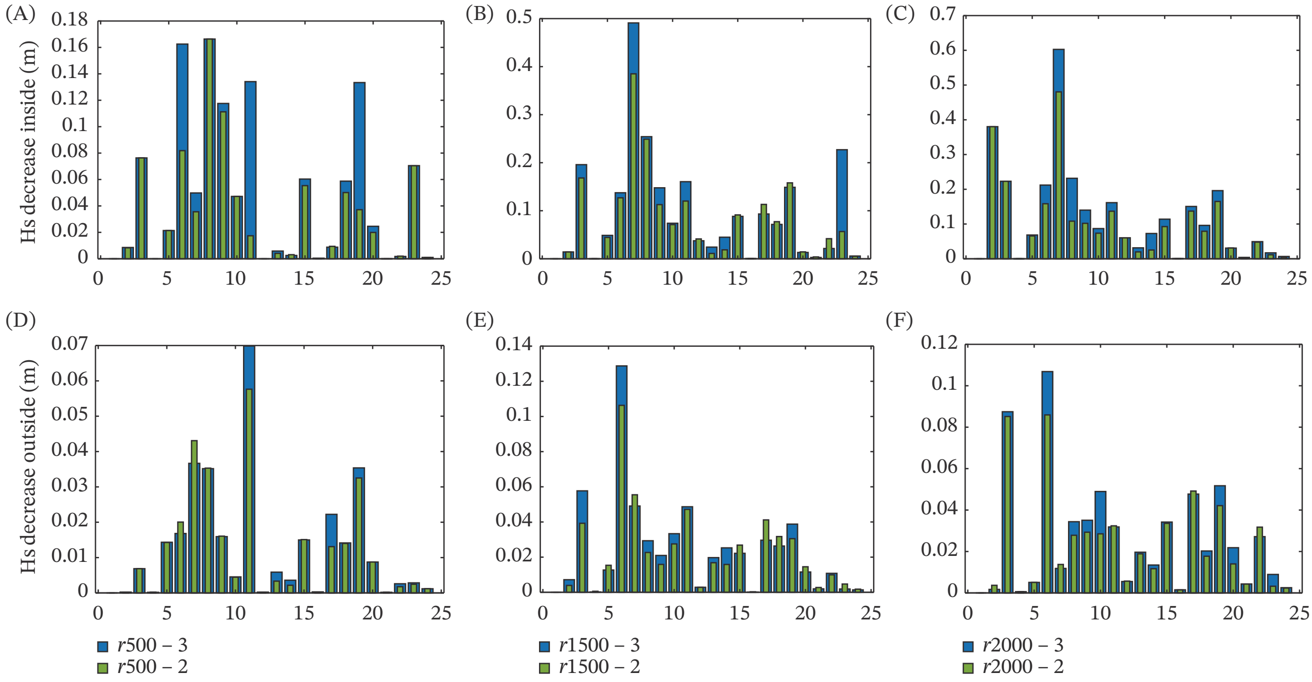


**FIGURE 5** | Decrease in significant wave height (m). The intervention number follows the numbering of Figure 1. This figure displays the maximum significant wave height dissipation (i.e., the difference between the maximum significant wave height before and after the intervention) recorded at any observation point within the intervention (A–C) or outside the intervention (D–F) for a wave height at the boundary Hs = 0.5 m.

shown in Figure 1. The results are presented for varying radii (500–2000 m) and intervention elevations (2 and 3 m).

Due to differences in coastline features and hydrodynamics along the coast, there is notable variability in wave dissipation along the horizontal axis. As the intervention diameter increases from 500 m to 1.5 and 2 km radius (Figure 5A–F), the reduction in maximum wave height at the site becomes more pronounced. Furthermore, the wave reduction associated with the intervention also intensifies with an increase in the intervention's elevation.

Significant reductions in wave height are observed at observation points located within the intervention area, whereas points outside the intervention (Figure 5D–F) experience only minimal changes. The wave height alterations in these external areas are substantially smaller, indicating that the interventions have a relatively limited impact on the surrounding wave field. Increasing intervention radius primarily modifies the cross-shore bathymetric gradient within the intervention area, promoting the earlier onset of depth-limited wave breaking and enhanced bottom frictional dissipation over the nourished zone. This explains why significant reductions in wave height occur at observation points within the intervention, while points outside experience only minimal changes. The more limited effect for points outside the interventions arises because wave energy is largely dissipated locally over the shallow nourishment platform, and remaining waves propagate beyond the feature with minimal further attenuation.

For observation points inside the intervention, for all but three (interventions 8, 9 and 23) interventions, increasing the radius from 500 m to 2 km, with a fixed elevation of 2 m, enhances the wave energy reduction potential. The larger reductions in wave height observed with an increased radius occur because a wider nourishment exposes waves to a larger shallow area, promoting greater energy dissipation. The largest effect is observed in intervention 7, where increasing the radius to 1.5 or 2 km results in an additional wave height reduction of 0.35 and 0.44 m, respectively, substantially higher than the 0.014 m increase achieved by raising the height alone. In contrast, for intervention 23, increasing the height from 2 to 3 m for a radius of 500 m produces no significant increase in maximum wave height reduction, whereas increasing the radius has a negative impact, with net changes of −0.0138 and −0.0590 m when increasing the radius to 1.5 km and 2 km, respectively.

On average, for observation points inside the intervention, increasing the radius from 500 m to 1.5 and 2 km results in maximum wave height reductions that are 0.046 m (0.053 m when neglecting interventions where the impact is negative) and 0.066 m (0.0857 m when neglecting interventions where the impact is negative) higher, respectively, compared with a 0.0139 m increase (0.022 m when neglecting interventions where the impact is negative) achieved by raising the height from 2 to 3 m for an intervention size of 500 m. When both the radius (from 500 m to 1.5 or 2 km) and height (from 2–3 m) are increased simultaneously, the average wave height dissipation rises by 0.0618 m (0.0677 m when neglecting interventions where the impact is negative) and 0.088 m (0.098 m when neglecting interventions where the impact is negative), respectively. These results indicate that, for most interventions, expanding the footprint is generally more effective than increasing elevation alone, although exceptions do occur when increasing the footprint or height has no positive impact. However, increasing the footprint radius is more effective for the 500 m intervention radius. Once the intervention radius is 1.5 km, increasing the radius from 1.5 to 2 km has mixed effects compared to increasing the height (Supporting Information 2 Figure S2).

Although the absolute variations in significant wave height across the interventions are modest (up to 0.6 m), such differences can be meaningful. Mega-nourishments are generally implemented as long-term sediment supply measures that enhance coastal resilience and support natural processes over decadal timescales. In most cases, they are not intended to function as primary flood defence structures in the manner of seawalls or embankments but rather to complement existing defences by improving morphological stability and reducing structural exposure. Within this framework, cumulative and low-intensity hydrodynamic effects become relevant for the long-term performance. Even moderate reductions in significant wave height, on the order of those observed in this study, translate into lower incident wave energy at the shoreline. Because wave energy scales with the square of wave height, these reductions correspond to measurable decreases in the hydraulic loading applied to both the nourishment body and any infrastructure situated landward. Reduced wave energy can limit erosion at the toe of embankments, decrease armour or revetment loading, and reduce the cumulative effects of repeated wave action over time. While such changes may not alter extreme design conditions, they are relevant for long-term maintenance and structural durability under frequent operating conditions. From a coastal engineering perspective, differences in wave height and water levels of this magnitude are also relevant for overtopping. Overtopping discharge depends non-linearly on the relative freeboard and incident wave height. Consequently, even small reductions in significant wave height can result in a disproportionate reduction in overtopping discharge under the same water level conditions. For low-crest systems operating near threshold conditions, this may shift the structure's response towards reduced overtopping discharge and potentially lower overtopping frequency under the same water level conditions. Although such changes may not redefine flood safety standards for low wave height, they can influence operational performance, exposure of materials to saline water, and long-term maintenance requirements.

In a similar fashion to Figure 5, Figure 6 represents the maximum differences in water levels before and after the implementation of a nourishment intervention for different radii of the intervention (different figures panels) and different intervention elevations (green and blue bars).

Figure 6A–C represent variations for observation points within the sand engine and Figure 6D–F are variations for observation points outside the sand engine. The location of the sand engine exerts a major influence on water level variations with significant site variability. For the observation points within the sand engine, the radius and height of the sand engine have a more evident impact on water level variations than for observation points outside the sand engine.

Similarly to wind waves, for the smaller intervention radius (500 m), increasing the intervention radius while maintaining the same intervention height generally leads to a greater reduction in water levels compared with increasing height alone. On average, an increase of 1 m in intervention height produces an additional reduction in maximum water levels within the intervention of 0.0078 m (0.025 m when neglecting interventions where increasing height has a negative impact). By contrast, increasing the radius from 500 m to 2 km results in an average reduction of 0.05 m (0.11 m when neglecting interventions where increasing height has a negative impact), while an intermediate radius increase to 1500 m yields an average reduction of 0.0218 m (0.067 m). Once the intervention radius is 1.5 km, increasing the radius from 1.5 to 2 km results in an increased reduction of 0.032 m (0.054 m), while increasing the height of the intervention 0.063 m (0.124 m), and trends are significantly more variable (Supporting Information 3 Figure S3). As for wave height reductions, there are cases where increasing the radius or height of the intervention has no positive impact.

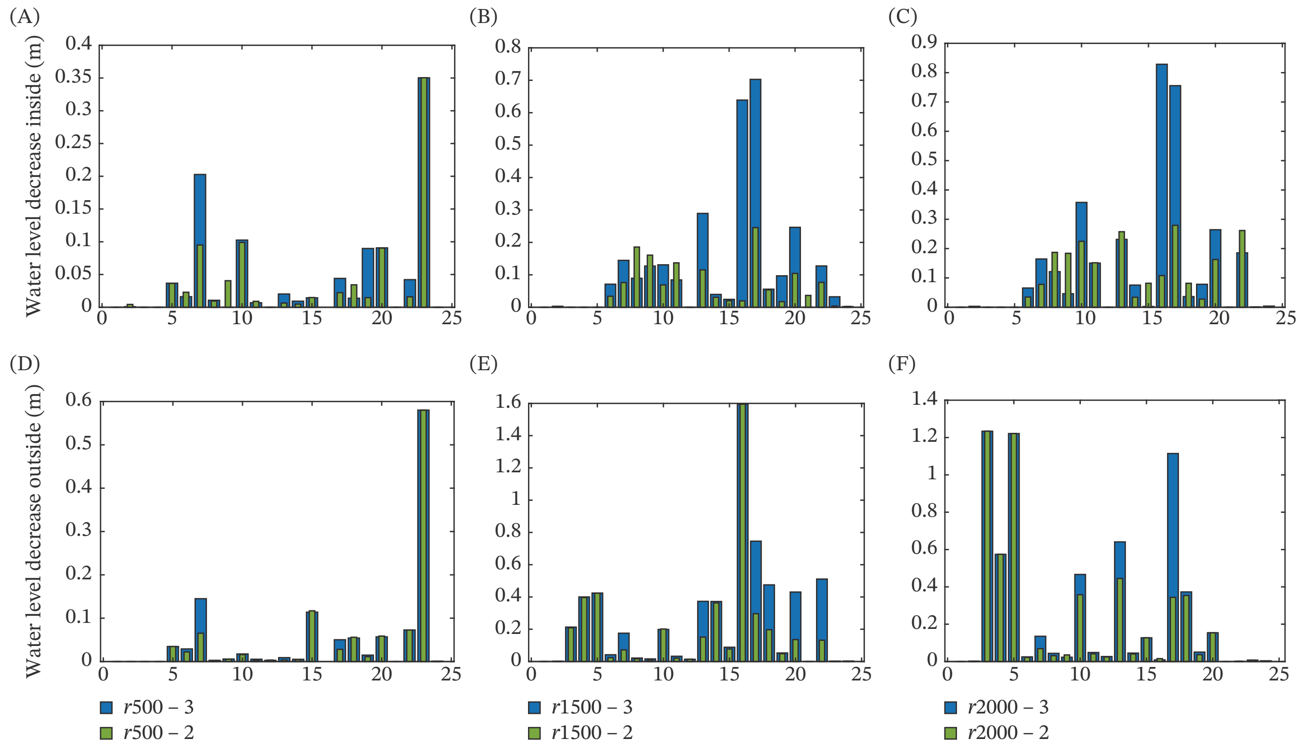


**FIGURE 6** | Decrease in water levels (m). Different colours indicate different sand engine elevations. The (A–C) refers to values obtained from observation points located within the intervention. The (D–F) refers to observation points located outside the intervention.

Figure 7 reports the maximum wave height reduction for observation points located within (Figure 7A) and outside (Figure 7B) the intervention and for different wave heights. Blue bars refer to simulations with a 0.5 m wave height imposed at the boundary. Orange bars refer to simulations with a 1 m wave height imposed at the boundary. Figure 7 highlights that the impact of the intervention in dissipating wave heights is enhanced when waves are higher (1 m rather than 0.5 m at the ocean boundary).

Studies such as Li et al. [35] show that during the evolution of a shoreface nourishment, wave energy dissipation is initially spatially variable, with peaks occurring over morphological features such as the seaward slope and inner bars. As the system evolves towards equilibrium, dissipation becomes more evenly distributed across the profile. This indicates that nourishment-induced bathymetric changes initially concentrate dissipation locally but over time promote a more uniform attenuation of wave energy across the nearshore zone. This behaviour is consistent with the present results, where dissipation is strongest over the intervention area and reflects the imposed bathymetric perturbation. Experimental work by Grasso et al. [36] highlights the so-called lee effect, whereby nourishments induce earlier wave breaking offshore. This shift in the breaking point enhances wave energy dissipation before waves reach the shoreline, thereby reducing the wave energy impacting the beach face. This mechanism aligns with the findings of the present study, where an increased intervention radius promotes earlier dissipation across the nourishment footprint. Johnson et al. [37] examine wave conditions over nearshore nourishment features, focusing on three configurations: linear berms, undulated berms, and discrete mounds. The study considers nourishments placed at depths between 3 and 7 m, with volumes of around 100,000 $m^3$ and alongshore extents ranging from 400 to 1000 m. Using numerical modelling, the authors analyse wave transformation, sediment transport and morphological response. As waves propagate from offshore towards the coast, they undergo shoaling, refraction and ultimately breaking, which are the key processes controlling energy dissipation. For the linear berm case, results show that when the feature is placed in relatively shallow water (around 3 m depth), waves begin to shoal and break further offshore, provided that they are large enough to interact with the seabed before reaching the natural breaking zone. This leads to changes in relative wave power of up to approximately $\pm 0.15$, particularly for configurations closest to the shore. At this shallow depth, the berm reduces wave energy flux across the area of interest (relative wave power $< 1$), with values dropping to around 0.75 in some cases. In contrast, when the berm is positioned deeper (5–7 m), waves are less affected, and relative wave power remains close to 1, indicating a negligible impact on wave transmission. The reduction in wave energy is also less pronounced for smaller waves as they are less sensitive to bathymetric changes. This is consistent with the smaller reduction in wave height observed in this study under lower-wave conditions.

## 4 | Conclusions

This article presents the results of numerical simulations conducted to explore the effectiveness of various coastal intervention types within a macro-tidal embayment. Specifically, the study focuses on the implementation of potential sand engines, based on simplified design configurations, to investigate trends in wave height and water level dissipation across different spatial scales. Coastal nourishment and mega-nourishment can serve not only as coastal protection measures but also as a means of supporting the development of natural habitats. In this numerical investigation, the interventions varied in size and location, with primary emphasis placed on reductions in significant wave height and water levels following large-scale coastal modifications. The case study considered is Morecambe Bay, a macro-tidal embayment located in the

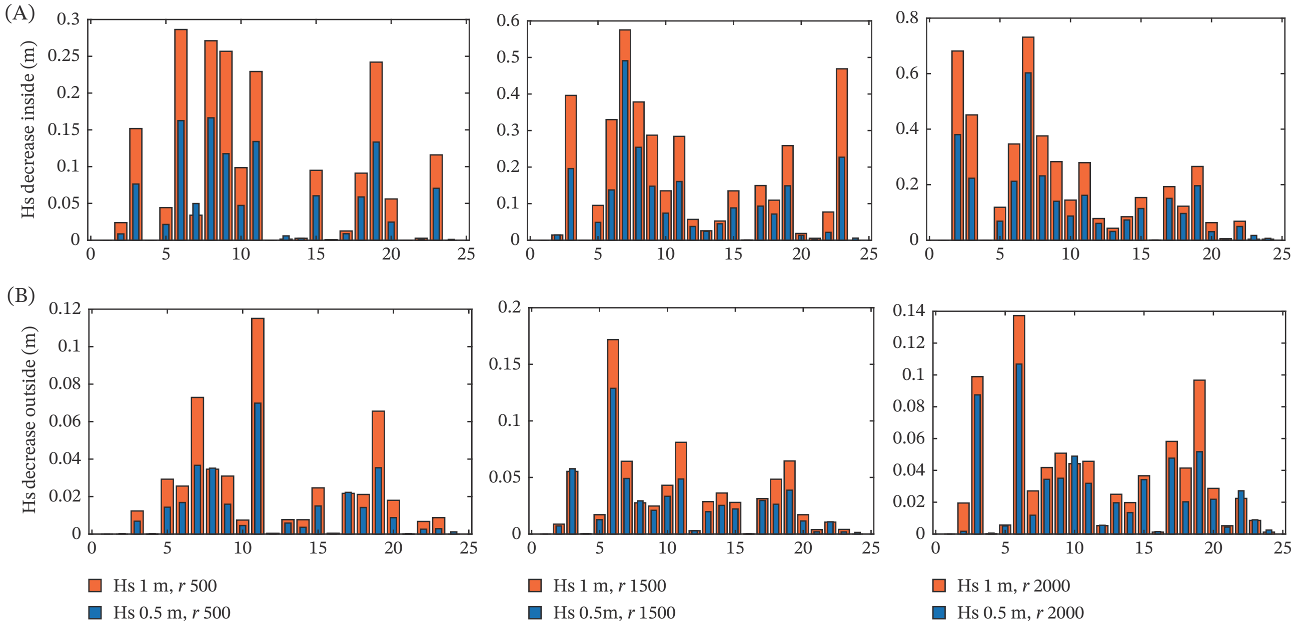


**FIGURE 7** | Decrease in significant wave height (m). Different colours indicate different wave heights at the model boundary (blue refers to 0.5 m significant wave height at the boundary; orange refers to 1 m wave height at the boundary). Results refer to a 3 m intervention height. The subpart (A) refers to values obtained from observation points located within the intervention. The subpart (B) refers to observation points located outside the intervention.

northwest of the UK. The findings from the numerical simulations suggest that:

- Overall, there is considerable variability in wave height dissipation across different intervention locations, as expected given the diverse shoreline characteristics within the model domain.
- Wave height dissipation due to the presence of the interventions is particularly pronounced during periods of high tide, reflecting the macro-tidal nature of the system (Figure 4).
- Increasing offshore wave height amplifies the impact of the interventions, leading to greater reductions in wave height (Figure 7).
- The size and characteristics of the interventions play a significant role in reducing significant wave height and water levels. For smaller radii (500 m), increasing the radius generally has a greater effect than increasing the intervention height. However, once the radius reaches ~1.5 km, further increases in radius produce mixed effects compared to increasing height (Figures 5 and 6).

There are limitations to the approach presented regarding the simplified geometric representation of the interventions. In reality, such interventions would exhibit spatially variable and evolving morphological characteristics that influence wave propagation and in situ wave dissipation. A real sand engine, for example, would typically undergo gradual spreading and lowering due to sediment redistribution, resulting in an increase in horizontal extent and a decrease in elevation over time. Based on the results of this study, this spreading is likely to extend the spatial footprint of wave energy dissipation, potentially providing protection over a wider coastal area. However, the reduction in elevation may decrease the localised effectiveness of the intervention in attenuating wave heights and water levels at specific points, particularly during higher-energy conditions. As suggested by the findings, increases in horizontal scale can enhance the overall impact up to a threshold, beyond which gains become less consistent. Therefore, the long-term performance of a sand engine is expected to involve a trade-off between reduced peak effectiveness and increased spatial coverage. Despite these limitations, this study provides useful insights that may serve as a starting point for coastal managers considering large-scale sand-scaping interventions in a range of coastal settings.


## Acknowledgments

This work was funded by EPSRC (Grant EP/V056042/1), EPSRC Engineering with Nature: combining artificial intelligence, remote sensing and computer models for the optimum design of coastal protection schemes. During the preparation of this work, the authors used ChatGPT (free version) in order to improve the readability and language of the manuscript.

## Funding

This work was funded by the Engineering and Physical Sciences Research Council (Grant EP/V056042/1).


## Disclosure

After using ChatGPT, the authors reviewed and edited the content as needed and take full responsibility for the content of the published article.

## Conflicts of Interest

The authors declare no conflicts of interest.

## Data Availability Statement

Bathymetry data have been retrieved from EDINA Marine Digimap (http://digimap.edina.ac.uk/, marine product download). The data for water levels and waves are from the Channel Coastal Observatory (https://coastalmonitoring.org/).

## References


1. R. J. Dawson, D. Johns, S. Gosling, et al., "UK Climate Change Risk Assessment Evidence Report: Chapter 4, Infrastructure," 2016, Report prepared for the Adaptation Sub-Committee of the Committee on Climate Change, London. 2016 https://www.theccc.org.uk/wp-content/uploads/2016/07/UK-CCRA-2017-Chapter-4-Infrastructure.pdf.

2. J. Maes and S. Jacobs, "Nature-Based Solutions for Europe's Sustainable Development," *Conservation Letters* 10, no. 1 (2017): 121–124.

3. R. L. Morris, T. M. Konlechner, M. Ghisalberti, and S. E. Swearer, "From Grey to Green: Efficacy of Eco-Engineering Solutions for Nature-Based Coastal Defence," *Global Change Biology* 24, no. 5 (2018): 1827–1842.

4. J. Forrester, N. Leonardi, J. R. Cooper, and P. Kumar, "Seagrass as a Nature-Based Solution for Coastal Protection," *Ecological Engineering* 206 (2024): 107316.

5. T. J. Bouma, J. Van Belzen, T. Balke, et al., "Identifying Knowledge Gaps Hampering Application of Intertidal Habitats in Coastal Protection: Opportunities & Steps to Take," *Coastal Engineering* 87 (2014): 147–157.

6. P. Kumar and N. Leonardi, "A Novel Framework for the Evaluation of Coastal Protection Schemes through Integration of Numerical Modelling and Artificial Intelligence into the Sand Engine App," *Scientific Reports* 13, no. 1 (2023): 8610.

7. P. Kumar and N. Leonardi, "Exploring Mega-Nourishment Interventions Using Long Short-Term Memory (LSTM) Models and the *Sand Engine Surface* MATLAB Framework," *Geophysical Research Letters* 51, no. 4 (2024): e2023GL106042.

8. N. Pannozzo and N. Leonardi, "Nature-Based Solutions for Coastal Protection: Untangling Public Knowledge and Perception across Europe," *Nature-Based Solutions* 9 (2026): 100297.

9. M. Schuerch, H. L. Mossman, H. E. Moore, E. Christie, and J. Kiesel, "Invited Perspectives: Managed Realignment as a Solution to Mitigate Coastal Flood Risks–optimizing Success Through Knowledge Co-Production," *Natural Hazards and Earth System Sciences* 22, no. 9 (2022): 2879–2890.

10. S. Rupp-Armstrong and R. J. Nicholls, "Coastal and Estuarine Retreat: A Comparison of the Application of Managed Realignment in England and Germany," *Journal of Coastal Research* 236 (2007): 1418–1430.

11. I. Möller, "Applying Uncertain Science to Nature-Based Coastal Protection: Lessons From Shallow Wetland-Dominated Shores," *Frontiers in Environmental Science* 7 (2019): 49.

12. L. Goeldner-Gianella, "Perceptions and Attitudes Toward De-polderisation in Europe: A Comparison of Five Opinion Surveys in France and the UK," *Journal of Coastal Research* 23, no. 5 (2007): 1218–1230.

13. J. Stronkhorst, B. Huisman, A. Giardino, G. Santinelli, and F. D. Santos, "Sand Nourishment Strategies to Mitigate Coastal Erosion and Sea Level Rise at the Coasts of Holland (the Netherlands) and Aveiro (Portugal) in the 21st Century," *Ocean & Coastal Management* 156 (2018): 266–276.

14. J. Arriaga, J. Rutten, F. Ribas, A. Falqués, and G. Ruessink, "Modeling the Longterm Diffusion and Feeding Capability of a Mega-Nourishment," *Coastal Engineering* 121 (2017): 1–13, 2017.

15. M. de Schipper, S. De Vries, G. Ruessink, et al., "Initial SpReading of a Mega Feeder Nourishment: Observations of the Sand Engine Pilot Project," *Coastal Engineering* 111 (2016): 23–38.

16. B. Roest, S. de Vries, M. de Schipper, and S. Aarninkhof, "Observed Changes of a Mega Feeder Nourishment in a Coastal Cell: 5 Years of Sand Engine Morphodynamics," *Journal of Marine Science and Engineering* 9, no. 1 (2021): 37.

17. A. P. Luijendijk, R. Ranasinghe, M. A. de Schipper, et al., "The Initial Morphological Response of the Sand Engine: A Process-Based Modelling Study," *Coastal Engineering* 119 (2017): 1–14.

18. E. Brand, G. Ramaekers, and Q. Lodder, "Dutch Experience With Sand Nourishments for Dynamic Coastline Conservation–An Operational Overview," *Ocean & Coastal Management* 217 (2022): 106008.

19. P. K. Tonnon, B. J. A. Huisman, G. N. Stam, and L. C. van Rijn, "Numerical Modelling of Erosion Rates, Life Span and Maintenance Volumes of Mega Nourishments," *Coastal Engineering* 131 (2018): 51–69.

20. T. Hudson, K. Keating, and A Pettit, "Cost Estimation for Coastal Protection – Summary of Evidence," (Environment Agency, 2015), https://assets.publishing.service.gov.uk/media/6034ee168fa8f5432c277c23/Cost_estimation_for_coastal_protection.pdf.

21. D. C. Mason and P. K. Garg, "Morphodynamic Modelling of Intertidal Sediment Transport in Morecambe Bay," *Estuarine, Coastal and Shelf Science* 53, no. 1 (2001): 79–92.

22. D. C. Mason, T. R. Scott, and S. L. Dance, "Remote Sensing of Intertidal Morphological Change in Morecambe Bay, UK, between 1991 and 2007," *Estuarine, Coastal and Shelf Science* 87, no. 3 (2010): 487–496.

23. A. W. Pringle, "Erosion of a Cyclic Saltmarsh in Morecambe Bay, North-West England," *Earth Surface Processes and Landforms* 20, no. 5 (1995): 387–405.

24. T. R. Scott and D. C. Mason, "Data Assimilation for a Coastal Area Morphodynamic Model: Morecambe Bay," *Coastal Engineering* 54, no. 2 (2007): 91–109.

25. L. M. Bricheno, D. Woolf, N. G. Valiente, N. Makrygianni, P. Chowdhury, and B. Timmermans, "Climate Change Impacts on Storms and Waves Relevant to the UK and Ireland," *MCCIP Science Review* 2025 (2025).

26. P. Kumar and N. Leonardi, "Coastal Forecast through Coupling of Artificial Intelligence and Hydro-Morphodynamical Modelling," *Coastal Engineering Journal* 65, no. 3 (2023): 450–469.

27. S. Putzu, F. Enrile, G. Besio, et al., "A Reasoned Comparison Between Two Hydrodynamic Models: Delft3D-Flow and ROMS (Regional Oceanic Modelling System)," *Journal of Marine Science and Engineering* 7, no. 12 (2019): 464.

28. L. Trinh Dinh and T. N. Viet, "Calibration and Verification of a Coupled Model for the Coastal and Estuaries in the Mekong River Delta, Vietnam," *Journal of Marine Science and Engineering* 14, no. 2 (2026): 157.

29. Y. Wu, E. Zhao, X. Li, and S. Zhang, "Application of Wave–current Coupled Sediment Transport Models with Variable Grain Properties for Coastal Morphodynamics: A Case Study of the Changhua River, Hainan," *Ocean Science* 21, no. 1 (2025): 473–495.

30. Deltares, "Delft3D-FLOW User Manual," 2026, https://content.oss.deltares.nl/delft3d4/Delft3D-FLOW_User_Manual.pdf.

31. R. D. Ray, "A Global Ocean Tide Model From Topex/Poseidon Altimetry: GOT99.2, NASA Tech Memo," (Goddard Space Flight Center: 581999, https://ntrs.nasa.gov/api/citations/19990089548/downloads/19990089548.pdf.

32. D. Stammer, R. D. Ray, O. B. Andersen, et al., "Accuracy Assessment of Global Barotropic Ocean Tide Models," *Reviews of Geophysics* 52, no. 3 (2014): 243–282.

33. Z. Defne and N. K. Ganju, "Quantifying the Residence Time and Flushing Characteristics of a Shallow, Back-Barrier Estuary: Application of Hydrodynamic and Particle Tracking Models," *Estuaries and Coasts* 38, no. 5 (2015): 1719–1734.

34. A. H. Murphy and E. S. Epstein, "Skill Scores and Correlation Coefficients in Model Verification," *Monthly Weather Review* 117, no. 3 (1989): 572–582.

35. Y. Li, C. Zhang, Y. Cai, M. Xie, H. Qi, and Y. Wang, "Wave Dissipation and Sediment Transport Patterns During Shoreface Nourishment Towards Equilibrium," *Journal of Marine Science and Engineering* 9, no. 5 (2021): 535.

36. F. Grasso, H. Michallet, and E. Barthélemy, "Experimental Simulation of Shoreface Nourishments under Storm Events: A Morphological, Hydrodynamic, and Sediment Grain Size Analysis," *Coastal Engineering* 58, no. 2 (2011): 184–193.

37. C. L. Johnson, B. C. McFall, D. R. Krafft, and M. E. Brown, "Sediment Transport and Morphological Response to Nearshore Nourishment Projects on Wave-Dominated Coasts," *Journal of Marine Science and Engineering* 9, no. 11 (2021): 1182.

## Supporting Information

Additional supporting information can be found online in the Supporting Information section. **Supporting Information 1**. The supporting file contains three figures showing the wave field, variations in wave height decrease, and variations in water level decrease. Figure S1. (A) Wave field for a wave height at the boundary of 1 m, at different instants of the tidal cycle: high tide (11:00:00), mean sea level (14:00:00) and low tide (17:00:00). **Supporting Information 2**. Figure S2. Variations in wave height decrease with increasing intervention size (m). The yellow bars represent the difference between the water level decrease caused by an intervention of radius 2 km and height 2 m and that caused by an intervention of radius 500 m and height 2 m. All decreases are calculated relative to the base scenario. The other bars are calculated in a similar manner. **Supporting Information 3**. Figure S3. Variations in water levels decrease with increasing intervention size (m). The yellow bars represent the difference between the water level decrease caused by an intervention of radius 2 km and height 2 m and that caused by an intervention of radius 500 m and height 2 m. All decreases are calculated relative to the base scenario. The other bars are calculated in a similar manner.